Original Article

Molecular Simulation Analysis of the Structure Complex of C2 Domains of DKK Family Members and β-propeller Domains of LRP5/6: Explaining Why DKK3 Does Not Bind to LRP5/6

Yasuyuki Fujii[a], Tyuji Hoshino[b], and Hiromi Kumon[a,c]*

[a]Innovation Center Okayama for Nanobio-Targeted Therapy, [c]Department of Urology, Okayama University Graduate School of Medicine, Dentistry and Pharmaceutical Sciences, Okayama 700–8558, Japan,
[b]Department of Physical Chemistry, Graduate School of Pharmaceutical Sciences, Chiba University, Chiba 260–8675, Japan

Dickkopf (DKK) proteins interact with low-density lipoprotein receptor-related protein 5/6 (LRP5/6) to modulate WNT signaling. The interaction is mediated by a cysteine-rich domain (C2) in the DKK protein and β-propeller domains (PD) of LRP5/6. However, the third member of the DKK family (DKK3) does not bind to LRP5/6. To determine why DKK3 does not bind to the receptor domains, we performed a molecular modeling simulation study including homology modeling, protein-protein docking and molecular dynamics (MD). The computed affinities ($\Delta G_{binding}$) between the C2 and PD models were consistent with the previously reported experimental results. The C2 model of DKK3 showed the lowest affinity for PD models. Multiple sequence alignment of C2 domains revealed that the DKK3 genes have a unique 7-amino-acid insertion (L249–E255 in human DKK3) and P258 in a finger loop 1 (FL1). Interestingly, the insertion sequence is evolutionally conserved. MD simulations of high-affinity complex models of C2 and PD showed that FL1 directly interacts with the PD models and stabilizes the complex models. We also built a 7-amino-acid-deletion/P258G mutant model of DKK3C2 and estimated its affinities for the PD models. The affinity for human LRP5PD2 was increased by the substitution ($\Delta G_{binding} = -48.9\,\mathrm{kcal/mol}$) and the affinity was compatible with that of high-affinity ligands. The results suggested that the lack of affinity between human DKK3 and human LRP5/6 results from: i) insertion of the 7 amino acids, and ii) P258 in human DKK3. The sequence differences thus suggest an explanation for this unique property of DKK3.

Key words: DKK3, molecular modeling, protein-protein docking, LRP5/6

The Dickkopf-3 (DKK3) protein was identified through the expression analysis of immortalized is also known as the REIC (reduced expression in immortalized cells) protein [1]. Expression of DKK3 is epigenetically suppressed in various types of carcinoma [2–13]. It has been revealed that DKK3 exerts

explicit tumoricidal activity [14–18] and anti-tumor immune response [19]. DKK family genes (DKK1–4) encode a pair of cysteine-rich domains (C1 and C2). The amino acid sequences of the C1 domains of DKK1 and DKK2 are 50% identical and those of the C2 domains are 70% identical [20]. The sequence similarity indicates that the C2 domain is more functionally important. In fact, the C2 domains of DKK1 and DKK2 have been shown to modulate WNT signaling [20]. It has also been shown that DKK4 weakly regu-

lates the WNT signaling [21]. The C2 domains directly bind to low-density lipoprotein receptor-related protein 5/6 (LRP5/6) for the regulation of WNT signaling [22–24]. However, DKK3 completely lacks affinity for LRP5/6 despite the presence of a C2 domain [25].

LRP5 plays critical roles in osteogenesis, including bone mass control via regulation of WNT signaling. Genotyping analysis has revealed that mutations in LRP5 induce high bone-mass disorders [26–30] and osteoporosis pseudoglioma syndrome [31]. Furthermore, depletion of LRP6 causes fatal defects in mouse embryos [32]. Mutations in human LRP6 (hLRP6) are associated with coronary artery disease and metabolic syndrome [33]. The binding regions of LRP5/6 for the C2 domain of DKK are located at the extracellular domain, which is composed of four 6-blade-type β-propeller units built by YWTD-EGF-like segments. The first β-propeller domain (PD1) of LRP5/6 is thought to be responsible for recognition of DKK [34, 35]. Interestingly, all of the mutations genetically linked to high bone-mass are located at the top surface of PD1 [30, 36, 37]. Recently, the crystal structures of a complex formed between hDKK1C2 and hLRP6PD3/4 have been determined [38, 39].

In the present study, we focused on the reason why DKK3 is unable to bind to LRP5/6. We considered that profiles of the affinities between C2 domains and PD would be helpful to answer this question. Chen *et al.* performed a protein-protein docking (PPD) simulation using a molecular model of mouse DKK2C2 (mDKK2C2) and hLRP6PDs [24]. In this study, we performed molecular simulations to predict the complex structures of C2 models in DKK proteins and PD models of LRP5/6 and to estimate their affinities.

Materials and Methods

The computational procedure for modeling the protein complex and affinity estimation is shown in Fig. 1. The details for each step are described below.

Homology modeling and refinement. The structure of the C2 domain of mDKK2C2 has been determined by NMR spectroscopy [24] (PDB code: 2JTK) and it was used as a model template for the C2 domains. The β-propeller domain of human low-density lipoprotein (LDL) receptor (PDB code: 1IJQ)
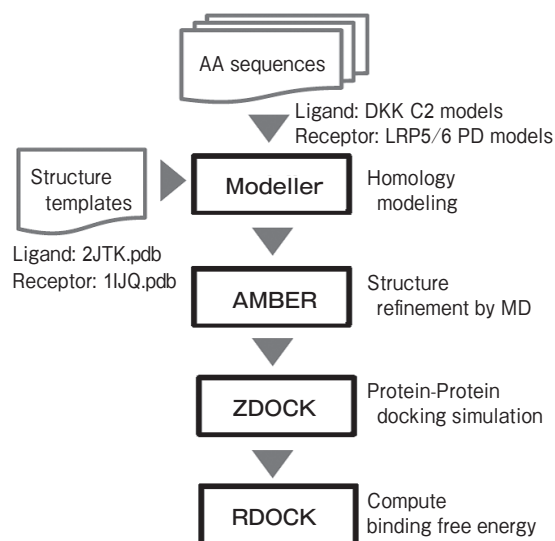

Fig. 1   Schemata of the prediction workflow used. After the computation, molecular dynamics (MD) simulations were performed on selected complex models to refine the structures and to obtain dynamic structures.

[40] was utilized as a model template for LRP5/6. Amino acid sequences of the C2 and β-propeller domains of LRP5/6 were extracted from the H-Invitational Database release 5.3 [41, 42] and UniProtKB/SwissProt [43]. The sequence IDs are listed in Table 1. Modeller 9v6 [44, 45] was used for homology modeling. The homology model with the lowest DOPE score [46] was used for the subsequent steps. To refine the homology models, energy minimization and molecular dynamics (MD) simulations were performed. TIP3P water [47] was used for an explicit solvent model. The force field used was Amber ff03. For energy minimization, the steepest descent and conjugated gradient methods were applied. The periodic boundary condition [48] was used in the simulated system to remove boundary effects. The cut-off distance of electrostatic interaction was 8 Å. The particle mesh Ewald [49] method was applied for computation of the energy of the Coulomb interaction. The integration time of an MD production run was 5 ns and the time step was 0.002 ps. AMBER10 was used for energy minimization and MD simulation.

Prediction of complex and binding energy. ZDOCK3.1 [50] was utilized for sampling complex models of C2 (as ligand) and PD (as receptor). The RDOCK/CHARMM system [51] was used to select

Table 1   Data sources for homology modeling. (A) The sequences IDs of human and mouse DKK1/2/3/4. (B) The sequence IDs of human and mouse LRP5/6. The regions listed are the targets for homology modeling. The %ID with the template (2JTK for DKKC2 and 1IJQ for LRP5/6PDs) and DOPE scores are also listed.

A

	Seq. ID	Modeled Region	%ID*	DOPE score
hDKK1C2	HIP000077490	K177–H266	65.9	−5158.9
hDKK2C2	HIP000022690	K171–I259	97.7	−5273.0
hDKK3C2	HIP000089868	K197–P286	31.3	−5802.9
hDKK4C2	HIP000109794	Q135–L224	56.1	−5048.8
mDKK1C2	O54908	K183–H272	63.2	−5032.9
mDKK3C2	Q9QUN9	Q197–P286	32.4	−5518.5
mDKK4C2	Q8VEJ3	S134–I221	55.4	−4995.3

*Sequence identity with template (PDB code: 2JTK)

B

	Seq. ID	Modeled Region	%ID**	DOPE score
hLRP5PD1		P33–A340	35.1	−31602.0
hLRP5PD2	HIP000044088	E342–E644	33.4	−31680.1
hLRP5PD3		V642–T945	28.8	−32787.0
hLRP5PD4		P943–P1257	23.8	−31993.3
hLRP6PD1		P21–D325	34.7	−31960.5
hLRP6PD2	HIP000054962	R340–P630	31.1	−29414.8
hLRP6PD3		P630–A931	33.0	−31929.8
hLRP6PD4		P932–E1245	25.3	−33624.8
mLRP5PD1		F36–A339	34.0	−30773.3
mLRP5PD2	Q91VN0	E341–P642	32.9	−31265.1
mLRP5PD3		P642–P942	30.2	−32532
mLRP5PD4		S944–E1254	23.0	−31866.1
mLRP6PD1		P21–D325	35.0	−32098.1
mLRP6PD2	O88572	R340–P630	30.1	−29716.7
mLRP6PD3		P630–A931	33.3	−31825.9
mLRP6PD4		P932–E1245	24.5	−32742.3

**Sequence identity with template (PDB code: 1IJQ)

the complex model with the highest affinity. $\Delta G_{binding}$ was used to estimate the affinity of the complex model. $\Delta G_{binding}$ is formulated using a combination of theoretical and empirical measures for binding energy and reflects the affinity of a protein-protein complex model. $\Delta G_{binding}$ is calculated by formula (1).

$$\Delta G_{binding} = \Delta G_{ACE} + \beta \times \Delta E_{elec} \quad (1)$$

ΔG_{ACE} denotes the atomic contact energy, which was empirically determined based on X-ray structure analysis [52]. β is a scaling factor for electrostatic energy and was set to 0.67 in this study. In the complex model sampling, the sides and bottom of PD models were blocked because the top surface of the PD domain is responsible for DKK recognition [34]. The contact surfaces were computed by MSMS [53].

Molecular dynamics simulation of the protein complex.   MD simulation was performed to obtain the equilibrium state of the solvated complex model. First, energy minimization was performed in a manner similar to that described above. Next, the system was gradually heated to 300 K for 320 ps. After the heating, the time step was changed to 0.002 ps for the following 100 ps and the thermodynamics ensemble was switched to NPT (isothermal-isobaric ensemble). Finally, a production MD run was carried out for 5 ns. The hydrogen bonds were counted if the averaged atomic distance was less than 4.0 Å or the minimum distance was less than 3.0 Å during the last 100 ps.

Multiple sequence alignment.   Multiple sequence alignment of the amino acid sequences of DKKC2 domains was generated with an online version of CLUSTALW [54] hosted by DDBJ [55]. The gap open penalty and extension penalty were 10.0 and 0.2, respectively.

Results

Dynamic structure of the C2 domains.   In order to model C2 domains under an aqueous condition, the molecular models were built by using a structural template of the solution structure of the mouse homolog [10] and refined by MD simulation using explicit solvent. Fig. 2 shows the dynamic structure of C2 models obtained in the MD simulation using an explicit solvent. The sequence identities (% ID) between the target and the model templates are shown in Table 1A. The C2 domains have 2 separated finger loops (FL1 and FL2). FL1 and FL2 are indicated by arrows in Fig. 2A, D, G and J. The dynamic structures show that FL1 and FL2 are more flexible than other parts of the C2 models. The root mean square displacement (RMSD) from the starting structure (Fig. 2B, E, H and K) shows that FL1 and FL2 in the models were equilibrated around 4 ns. The atomic fluctuations (Fig. 2C, F, I and L) show that the motion of FL1 in hDKK2C2 (T215–Q229) was greater than that in other regions. This result is consistent with the results of NMR spectroscopy of mDKK2C2 [24]. FL1 of hDKK3C2 was longer than those of other C2 models due to a conserved 7-amino-acid insertion (LDLITWE) unique to DKK3 (Fig. 3). Hence, FL1 in DKK3C2 shows higher flexibility because of the unique insertion. FL1 of hDKK3 and

that of hDKK4 were twisted (Fig. 2G and J). It should be noted that the C2 domains in hDKK3 and hDKK4 contain a proline residue (P258 in hDKK3 and P188 in hDKK4) at FL1 (see the alignment in Fig. 3). The proline residue is able to restrict conformation of the main chain due to its rigid cyclic structure. Hence, we speculated that the twist of the loop is caused by the proline residue in hDKK3 and hDKK4 and that the conformation influences the affinity for LRP5/6. In fact, the agonistic effect of DKK4 on WNT signaling has been reported to be marginal compared with the agonistic effects of DKK1 and DKK2 [21]. As described above, DKK3 does not bind to LRP5/6. Therefore, it is thought that the lower affinity of DKK3 and DKK4 to LRP5/6 is due to the twisted conformation in FL1.

Dynamic structures of molecular models of the β-propeller domains in LRP5/6. The sequence alignments of the template (PDB code: 1IJQ) and LRP5/6PDs show that the sequence identities ranged from 24% to 35% (Table 1B). In the homology modeling, 3 intermolecular disulfide bonds in the EGF-like domain of PD models were constructed on the basis of the model template. The computed dynamic structures of hLRP5PD1 to PD4 are depicted in Fig. 4A, C, E, and G. According to the atomic fluctuations in the equilibrium state (Fig. 4B, D, F, and H), the conformation was rigidly maintained in all of the PD models except for the EGF-like domains. Although several N-linked glycosylation sites were predicted on β-propeller domains of hLRP5/6, all of the glycosides were omitted in the molecular models. Therefore, the simulation results indicated that glycosylation is not important for the stability of β-propeller domains. In the dynamic structures of the PD1, PD2 and PD3 models of hLRP5, the atomic fluctuations of EGF-like domains were greater than those of β-propeller domains (Fig. 4B, D and F). According to their dynamic structures (Fig. 4A, C and E), the overall structures of EGF-like domains were not disordered. The flexibility of the EGF-like domains seemed to be restricted by the disulfide bonds in their interiors. These dynamic properties were also observed in the MD simulation for PD models of hLRP6 and the same series of mouse models (data not shown). The final structures of PD models in MD simulations were used as receptors in the following PPD simulation.

Prediction of complex structures and affinities of DKK ligands and receptors. The affinity profiles of the predicted complexes are shown in Table 2. Based on the profile of the human model series (Table 2A), the complex model with the highest affinity was hDKK1C2–hLRP6PD1 ($\Delta G_{binding} = -56.6$ kcal/mol). This is consistent with the result of an experimental study showing that the C2 domain of DKK1 is directly bound to PD1 of LRP6 [56]. In the complex model of hDKK1C2–hLRP6PD1, 51 hydrogen bonds were detected. The contact surface area was 3,960 Å². According to the statistics on 75 protein-protein complexes, the contact surface ranges from 1,150 to 4,660 Å² [57]. Hence, the complex is cooperatively maintained by the hydrogen bond network (HBN) and the broad contact surface. Binnerts *et al.* suggested that Ser243 in PD1 of hLRP6 was important for binding to DKK1 [56]. In our predicted complex model, the hydroxyl group of Ser243 was involved in hydrogen bonds with atoms in Cys201 of hDKK1. The atomic distances of Cys201O–Ser243OG and Cys201N–Ser243OG were 2.67 Å and 3.23 Å, respectively. This means that Cys201 and Ser243 are associated by 2 hydrogen bonds. The computed $\Delta G_{binding}$ of hDKK1C2–hLRP6PD3 was −48.0 kcal/mol. The crystal structure of the complex has been independently determined by 2 groups [38, 39]. In both crystal structures (PDB code: 3S8V and 3S2K), one engineered protein from hDKK1C2 and 2 proteins from hLRP6PD3/4 are included in a unit cell of the crystal. Hence, it has been observed in these crystallographic studies that one hDDK1 protein makes 2 different contacts with the hLRP6 proteins. It is natural to consider that one of the hDDK1–hLRP6 contacts observed in the crystal structure is biologically relevant but the other is accidentally formed in the process of protein crystallization. Our predicted binding mode of hDKK1C2–hLRP6PD3 showed a significant structural similarity with one of the contacts observed in the crystals. The superimposed structures between the predicted complex model and crystal structure are depicted in Fig. 5. The root mean square (RMS) deviations for Cα of our predicted structure against 3S8V and 3S2K were 4.18 Å and 3.96 Å, respectively. The other contact observed in the crystals was dissimilar with our predicted binding mode (RMS deviation for Cα ≥ 8 Å). The good accordance with the experimental results suggests that our
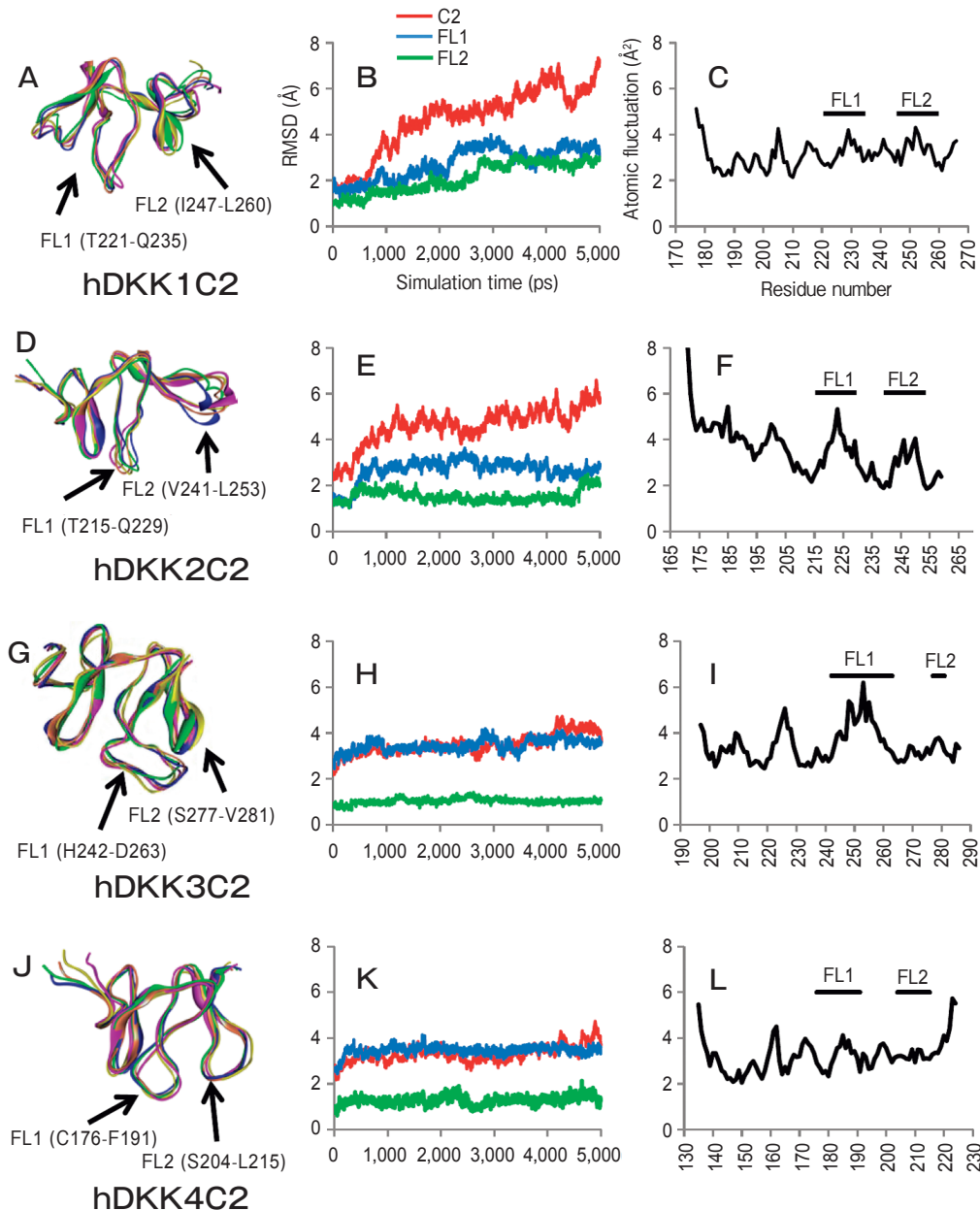
Fig. 2 Computational results of MD simulation for the modeled C2 domains of human DKK proteins. **A**, **D**, **G** and **J** are dynamic structures that are represented by an overlap of snapshots from the MD simulations. The flexible loops (FL) in each structure are indicated by arrows. The colors in the structures indicate the duration of the snapshot. Green: 1 ns; blue: 2 ns; orange: 3 ns; pink: 4 ns; yellow: 5 ns. **B**, **E**, **H** and **K** shown the time-course development of RMSD values in the MD simulations. The plots colored in red, blue and green indicate the full structures of C2 models, FL1 and FL2, respectively. **C**, **F**, **I** and **L** show the atomic fluctuations of the peptide backbone by residue in MD simulations. The regions of the FL loops are indicated by lines. The graphics of the protein-protein complex models are depicted using Discovery Studio 2.5 (http://accelrys.com/events/webinars/discovery-studio-25/).

prediction approach is reasonable.

It should be noted that $\Delta G_{binding}$ of the hDKK3C2 model and PD models of LRP5 or 6 ranked the worst among the DKK models. For example, the computed affinity of the hDKK3C2 model and hLRP5PD2 model ($\Delta G_{binding} = -31.2\,kcal/mol$) was the lowest among the

A

```
hDDK1C2  1 KMYHTKGQEGSVCLRSSDCASGLCCA--RHFWSKICKPVLKEGQVCTKHRRKG-------
mDKK1C2  1 KIYHTKGQEGSVCLRSSDCAAGLCCA--RHFWSKICKPVLKEGQVCTKHKRKG-------
hDKK2C2  1 KMSHIKGHEGDPCLRSSDCIEGFCCA--RHFWTKICKPVLHQGEVCTKQRRKG-------
mDKK2C2  1 -MPHIKGHEGDPCLRSSDCIDGFCCA--RHFWTKICKPVLHQGEVCTKQRRKG-------
hDKK4C2  1 --QGRKGQEGESCLRTFDCGPGLCCA--RHFWTKICKPVLLEGQVCSRRGHKDT------
mDKK4C2  1 -SQSSKGQEGESCLRTSDCGPGLCCA--RHFWTKICKPVLEEGQVCSRRGHKDT------
hDKK3C2  1 -KMATRGSNGTICDNQRDCQPGLCCAFQRGLLFPVCTPLPVEGELCHDPASRLLDLITWE
mDKK3C2  1 -QKATKGGNGTICDNQRDCQPGLCCAFQRGLLFPVCTPLPVEGELCHDPTSQLLDLITWE
```

```
hDKK1C2  52 SHGLEIFQRCYCGEGLSCRIQKDHHQASNSSRLHTCQRH
mDKK1C2  52 SHGLEIFQRCYCGEGLACRIQKDHHQASNSSRLHTCQRH
hDKK2C2  52 SHGLEIFQRCDCAKGLSCKVWKDATYSS-KARLHVCQKI
mDKK2C2  51 SHGLEIFQRCDCAKGLSCKVWKDATYSS-KARLHVCQKI
hDKK4C2  51 AQAPEIFQRCDCGPGLLCRSQLTSNRQH--ARLRVCQKI
mDKK4C2  52 AQAPEIFQRCDCGPGLLCRSQVTSNRQH--SRLRVCQKI
hDKK3C2  60 LEPDGALDRCPCASGLLCQP-----HSH--SLVYVCKPT
mDKK3C2  60 LEPEGALDRCPCASGLLCQP-----HSH--SLVYMCKPA
```

B

```
             180         190         200         210         220
hDDK1C2  KMYHTKGQEGSVCLRSSDCASGLCCA--RHFWSKICKPVLKEGQVCTKHRRKG-------

             180         190         200         210         220
hDKK2C2  KMSHIKGHEGDPCLRSSDCIEGFCCA--RHFWTKICKPVLHQGEVCTKQRRKG-------

             140         150         160         170         180
hDKK4C2  --QGRKGQEGESCLRTFDCGPGLCCA--RHFWTKICKPVLLEGQVCSRRGHKDT------

             200         210         220         230         240         250
hDKK3C2  -KMATRGSNGTICDNQRDCQPGLCCAFQRGLLFPVCTPLPVEGELCHDPASRLLDLITWE
```

```
             230         240         250         260
hDKK1C2  SHGLEIFQRCYCGEGLSCRIQKDHHQASNSSRLHTCQRH

             230         240         250
hDKK2C2  SHGLEIFQRCDCAKGLSCKVWKDATYSS-KARLHVCQKI

             190         200         210         220
hDKK4C2  AQAPEIFQRCDCGPGLLCRSQLTSNRQH--ARLRVCQKI

             260         270         280
hDKK3C2  LEPDGALDRCPCASGLLCQP-----HSH--SLVYVCKPT
```
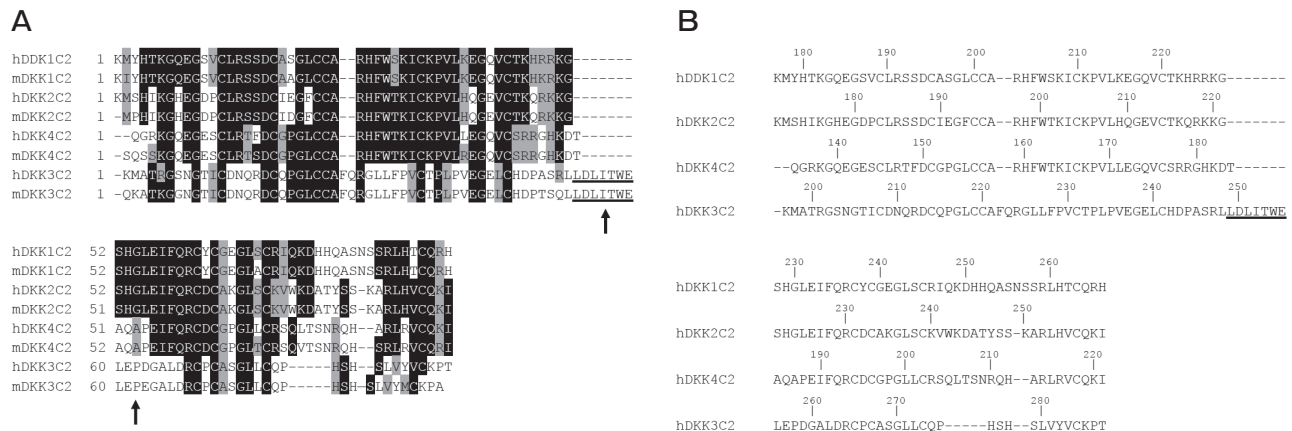
Fig. 3 A, Multiple alignments of the C2 domains in human and mouse DKK proteins. The conserved amino acid residues are represented by the black letters. The non-conserved residues that maintain a similar polar property are shown with a gray background. The amino acid insertion unique to DKK3 and Pro258 and that observed only in DKK3 are indicated by arrows; B, Amino acid sequences of the C2 domains in human DKK proteins.

C2 complexes with hLRP5PD2. This result means that hDKK3 has the lowest affinity among the DKK proteins. This tendency was also observed in the affinity profiles of mouse models (Table 2B). Judging from the above, hDKK3 and mDKK3 have less affinity for the LRP receptors, which is consistent with the experimental results. Fig. 6 shows the binding modes found in the complex model of C2 and hLRP5PD2. Although the binding modes were dissimilar, FL1 and FL2 in the C2 models of DKK1/2/4 are in direct contact with the top of the β-propeller domain. According to the crystal structures of hDKK1C2 and hLRP6PD3, FL1 of hDKK1C2 was directly attached to the top surface of the PD domain [38, 39]. This also supports our results in the complex prediction. In contrast, FL1 of the hDKK3C2 model was not in contact with the hLRP5PD2 model. This unusual binding mode may result from the additional 7-amino-acid sequence unique to DKK3.

Dynamic properties of the interaction in high-affinity complexes

1. Contribution of FL1 and FL2 in the hDKK1C2–LRP6PD1 complex model. According to the affinity profile, the hDKK1C2–hLRP6PD1 complex model has the highest affinity among the human models ($\Delta G_{binding} = -56.6$ kcal/mol). To elucidate the dynamic properties and persistence of HBN found in the complex model, MD simulation was performed. Fig. 7A shows the dynamic structure of hDKK1C2 in the complex model in the equilibrium

state. According to the dynamic structure, FL1 maintained tight contact with the top surface of the hLRP6PD1 model. Fig. 7B shows the RMSD during the MD simulation. The RMSD of the complex model shows that the system was equilibrated sufficiently. It also shows that the dynamics of the receptor-free model of hDKK1C2 compared well with that of the complex. This means that hDKK1C2 is dramatically stabilized by the association with hLRP6PD1. Fig. 7C shows the atomic fluctuations of residues in the PD-bound and unbound hDKK1C2 models. The atomic motions of hDKK1C2 in the complex were smaller in all of the residues. This also indicates that the receptor binding enhances the stability of the C2 domain. In particular, 3 separate regions consisting of C195–H204, S207–H224 and R236–Q248 in the hDKK1C2 model were strongly stabilized by the receptor binding. It is interesting to note that most parts of the stabilized regions were outside of FL1 (T221–Q235) and FL2 (I247–L260) in hDKK1C2. This suggests that not only FL1 and FL2 but also other regions contribute to formation of the complex. Indeed, as shown in Table 3, the HBN between hDKK1C2 and hLRP6/5PD1 was observed not only at the FL1 and FL2 but also at the regions outside of FL1 and FL2. Sixty-six hydrogen bonds were found in the equilibrated state of the complex model. Twenty-four of those hydrogen bonds were thought to persist in the equilibrated state because the averages of their atomic distances over the preceding 100 ps were less than
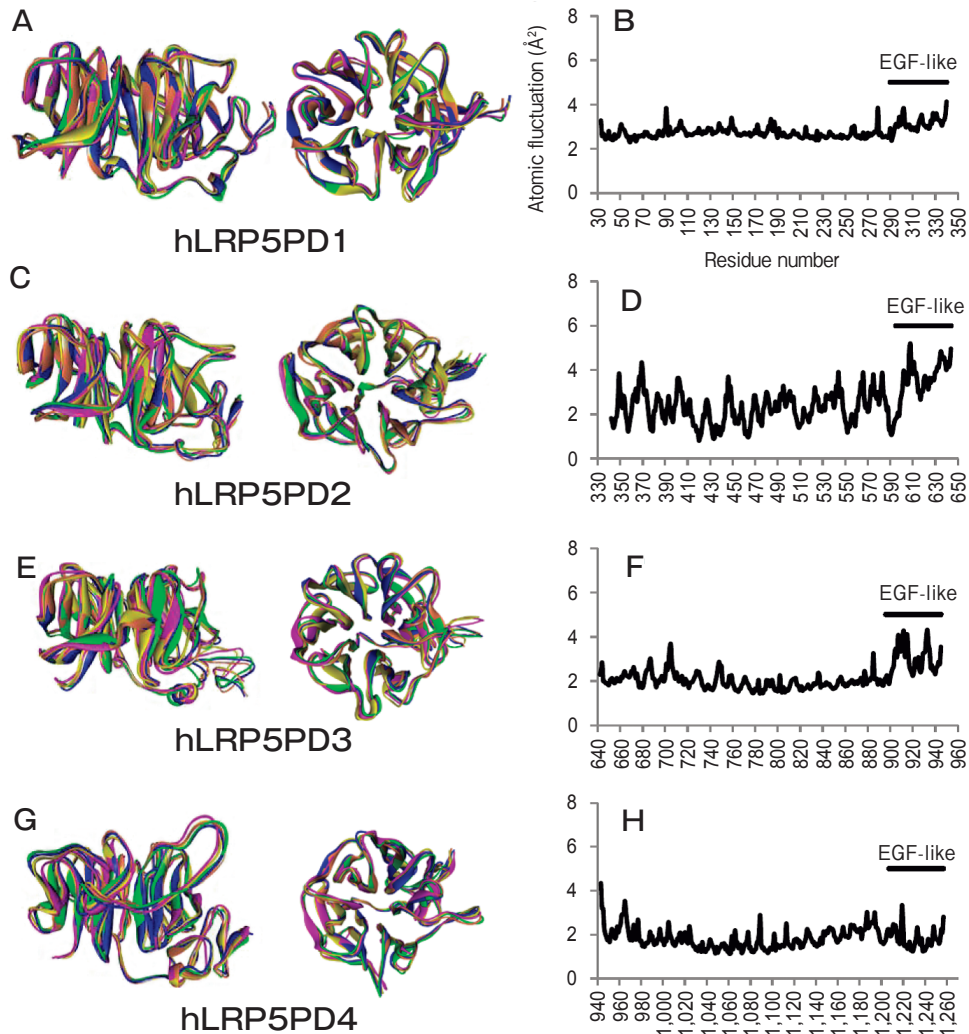
Fig. 4 Dynamic structures of the modeled β-propeller domains (PD) in hLRP5 proteins. **A**, **C**, **E** and **G** are dynamic structures of PD1, 2, 3 and 4, respectively. Top (right) and side (left) views are shown. The snapshot structures are colored in the same manner as those in Fig. 2. **B**, **D**, **F** and **H** are atomic fluctuations of the backbone by residue in MD simulations.
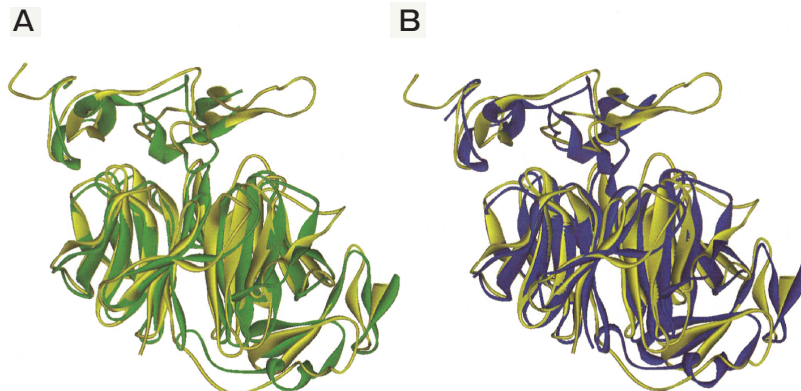

Fig. 5 **A**, Overlapped structure of crystallized 〔light green, PDB code: 3S8V (Cheng *et al.* 2011)〕 and our predicted structure of hDKK1C2–hLRP6PD3 (yellow). The RMS deviation between the structures was 3.96Å; **B**, Overlapped structure of crystallized 〔purple, PDB code: 3S2K (Ahn *et al.* 2011)〕 and our predicted complex of hDKK1C2–hLRP6PD3 (yellow). The RMS deviation between the structures was 4.18Å.

hDKK1C2-hLRP5PD2   hDKK2C2-hLRP5PD2

hDKK3C2-hLRP5PD2   hDKK4C2-hLRP5PD2
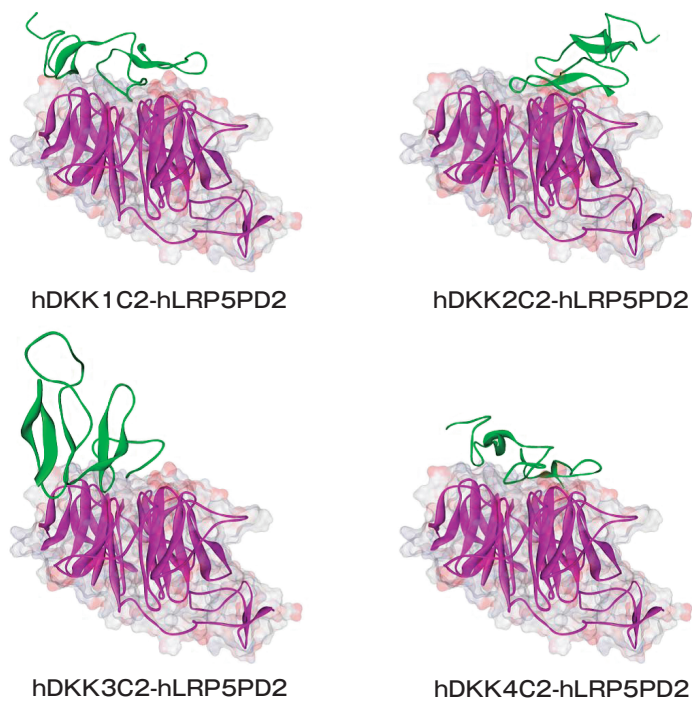
Fig. 6   Predicted complex models of the C2 domains in hDKKs and hLRP5PD2 predicted by protein-protein docking simulations.
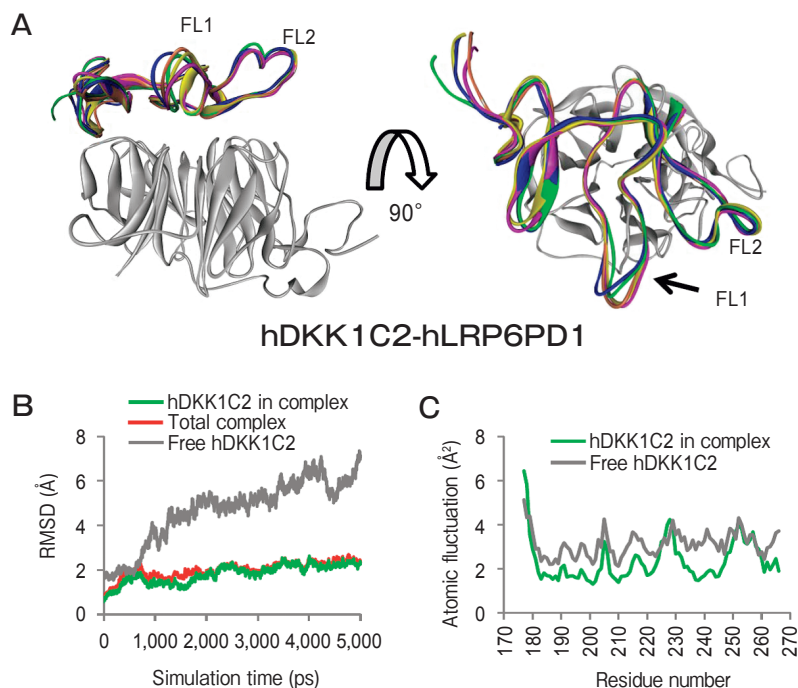

Fig. 7   A, Complex model of hDKK1C2–hLRP6PD1. The dynamic structure of the hDKK1C2 model, which was obtained by MD simulation, is represented on the left. The dynamic structure is colored in the same manner as that in Fig. 2. A 90° rotated view of the complex model is also depicted to show the receptor recognition position of hDKK1C2 (right); **B,** Time-course development of the RMSD values in MD simulations of the complex model and free hDKK1C2. The plots in green, red and gray indicate hDKK1C2, hLR-P6PD1 in the complex model, and free hDKK1C2, respectively; **C,** Atomic fluctuation of the peptide backbone in hDKK1C2. The plots in green and gray indicate hDKK1C2 in the complex and free form, respectively.

4.0Å.

2. Significance of FL1 in the hDKK1C2–LRP5PD1 model. In biochemical experiments on WNT signaling, hDKK1 is frequently used as an antagonist for hLRP5 due to its effective inhibitory response. The interaction between hDKK1 and hLRP5 has been characterized in experimental studies using mutation analyses. Several mutations in hLRP5 were

Table 2 Affinity profile of the complex models consisting of human (A) or mouse (B) C2 domains of DKK ligand and PD domains of LRP5 and 6. The values shown are in kcal/mol.

A

$\Delta G_{binding}$	hDKK1C2	hDKK2C2	hDKK3C2	hDKK4C2
hLRP5PD1	−47.70	−50.56	−29.33	−40.21
hLRP5PD2	−56.02	−55.25	−31.22	−47.95
hLRP5PD3	−42.90	−36.42	−28.64	−43.43
hLRP5PD4	−29.07	−30.99	−24.97	−19.77
hLRP6PD1	−56.57	−34.02	−27.63	−44.89
hLRP6PD2	−44.54	−36.72	−32.41	−38.42
hLRP6PD3	−48.57	−31.43	−22.89	−21.15
hLRP6PD4	−28.20	−26.95	−31.51	−25.96

B

$\Delta G_{binding}$	mDKK1C2	mDKK2C2	mDKK3C2	mDKK4C2
mLRP5PD1	−47.75	−51.38	−37.07	−70.50
mLRP5PD2	−46.79	−45.76	−44.03	−47.19
mLRP5PD3	−33.26	−34.48	−25.38	−37.24
mLRP5PD4	−40.46	−30.57	−35.43	−35.06
mLRP6PD1	−42.99	−36.36	−26.29	−50.79
mLRP6PD2	−43.48	−56.72	−39.09	−56.43
mLRP6PD3	−36.90	−35.66	−29.59	−33.09
mLRP6PD4	−34.02	−27.66	−34.37	−23.83

Unit is kcal/mol.

Table 3 The stable hydrogen bonds observed in the equilibrium state of dynamic structures of the complex models, hDKK1C2–hLRP6PD1 (A) and hDKK1C2–hLRP5PD1 (B). The averaged atomic distances and their standard deviation (S.D.) are shown along with the min/max distances observed during the last 100 ps of MD simulation on the complex models. The values shown are in Å.

A

hDKK1C2–hLRP6PD1	Average	S.D.	Minimum	Maximum
H180N–T328O	2.25	0.01	2.11	2.40
E232O–R29NH1	2.85	0.02	2.57	3.76
H223NE2–E115OE1	2.87	0.02	2.60	3.48
K222NZ–ASP98OD1	2.91	0.04	2.56	4.03
K222NZ–S96O	2.99	0.04	2.60	4.02
R224O–R29NH1	3.05	0.13	2.64	4.70
S244OG–Q139NE2	3.10	0.09	2.69	4.70
E241OE2–K202NZ	3.11	0.21	2.58	4.94
R203NE–I265O	3.18	0.07	2.62	4.32
E241OE1–K202NZ	3.18	0.27	2.60	5.11
K222NZ–P97O	3.18	0.13	2.54	4.78
K222NZ–D98OD2	3.26	0.22	2.64	4.91
H266NE2–W157O	3.27	0.15	2.66	5.38
C201O–H245NE2	3.35	0.22	2.64	5.40
K249NZ–E115O	3.43	0.71	2.60	7.21
K222NZ–S96OG	3.44	0.12	2.66	4.49
Q235OE1–S267N	3.52	0.26	2.69	5.65
S244OG–Q139OE1	3.57	0.22	2.41	4.68
K208NZ–T244O	3.58	0.34	2.60	5.23
Y238OH–A201O	3.68	0.42	2.58	6.04
C245N–W157NE1	3.70	0.11	2.94	4.67
A202O–H245NE2	3.75	0.13	2.86	5.23
R224O–R29NH2	3.77	0.23	2.82	5.22
R203NH2–I265O	3.79	0.17	2.79	5.05
R203NH2–D264O	3.86	0.75	2.65	6.85
H180N–A327O	3.87	0.17	3.05	5.26

Unit is Å.

B

hDKK1C2–hLRP5PD1	Average	S.D.	Minimum	Maximum
K222NZ–E128OE2	2.86	0.03	2.58	3.62
R203NH2–Y195O	2.91	0.02	2.62	3.40
S207O–Y195OH	2.97	0.07	2.53	4.44
S228O–S280N	3.06	0.10	2.64	4.90
K222NZ–E128OE1	3.14	0.14	2.54	4.34
L231O–W255NE1	3.23	0.13	2.61	4.67
R203NH1–W170O	3.28	0.15	2.64	4.53
W206NE1–K215O	3.42	0.62	2.63	7.90
S207N–Y195OH	3.46	0.06	2.86	4.97
H229O–W255NE1	3.52	0.25	2.69	5.94
R203NH1–Y195O	3.57	0.33	2.68	5.27
H204O–Y195OH	3.61	0.11	2.75	5.15
H204N–Y195OH	3.62	0.11	2.89	5.73
F205O–Y195OH	3.63	0.14	2.88	5.40
R203NE–Y195OH	3.80	0.12	2.70	5.06
R203NH2–W170O	3.86	0.21	2.81	5.18
K222NZ–S109OG	3.87	0.25	2.87	6.73
H229O–S280N	3.92	0.16	2.67	5.31
S228O–R258NE	3.92	0.24	2.84	5.36
R203NH1–G171O	3.93	0.34	2.75	6.00
G230N–S280OG	3.94	0.09	3.20	5.13
A203NH2–W196NE1	3.99	0.18	3.20	6.20

Unit is Å.

detected on the first propeller domain of hLRP5 [28, 30, 37]. The mutations were reported to reduce the affinity for DKK1. In order to determine the protein-protein interactions contributing to the affinity, MD simulation of the hDKK1C2–hLRP5PD1 complex model was performed. Similar to that of the hDKK1C2–hLRP6PD1 model, the molecular motion of the hDKK1C2 model was stabilized by binding to the hLRP5PD1 model (Fig. 8C). The difference in the molecular motion of hDKK1C2 between the complex model with hLRP5PD1 and that with hLRP6PD1 was explained by comparing the binding mode and contact surface areas as follows. In the complex model of hDKK1C2–hLRP6PD1, FL1 and FL2 of hDKK1C2 are in contact with the top surface of hLRP6PD1 (Fig. 7A). In the hDKK1C2–hLRP5PD1 model, only FL1 attaches to hLRP5PD1 (Fig. 8A). The contact surface areas of the hDKK1C2–hLRP6PD1 and hDKK1C2–hLRP5PD1 complex models were $3,960 \text{Å}^2$ and $2,627 \text{Å}^2$, respectively. This means that FL1 is essential for binding to the PD domain and FL2 assists in further stabilization of the protein complex.

The total number of stable hydrogen bonds observed in the equilibrium state of the complex model was 39. This means that the complex model is stabi-lized by HBN. FL1 in DKK1C2 was responsible for 33 hydrogen bonds in the complex model. This means that more than half of the intermolecular hydrogen bonds in the complex model were produced by FL1. Hence, it can be concluded that the hydrogen bonds provided by FL1 significantly contribute to the inter-action of hDKK1C2 and hLRP5PD1 (Table 3B). Although the contact interface of the complex model is relatively narrow, the HBN effectively stabilized the whole structure of the complex. In addition, a number of weak hydrogen bonds also contributed to the stabi-lization of the complex (Table 4B). The inhibitory level in WNT signaling by the DKK ligand is consid-ered to be correlated with the stability of interaction between the C2 domain and PD domain.

Insertions/substitutions unique to DKK3 and their influence on the binding affinity to LRP5.   It is important to address the reason why DKK3 does not bind to PD domains. As previously mentioned, a conserved insertion (LDLITWE), which is unique to both human and mouse DKK3C2, was found in the multiple sequence alignment (Fig. 3). In the homology models of DKK3C2, the conserved regions were found in the FL1 region. MD simulation of the complex model of hDKK1C2–hLRP5PD1
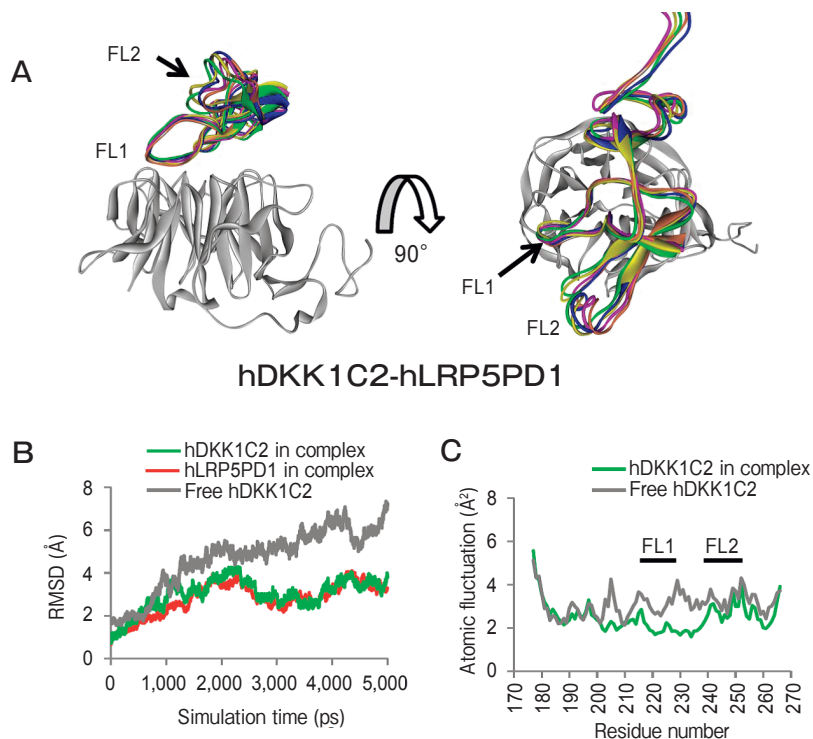

hDKK1C2-hLRP5PD1

Fig. 8   **A**, The complex model of hDKK1C2–hLRP5PD1; **B**, Time-course development of the RMSD values in the MD simulations. The plots in green, red and gray indicate hDKK1C2, hLRP5PD1 in the complex model, and free hDKK1C2 model, respectively; **C**, Atomic fluctuation of the peptide backbone in the hDKK1C2 model. The plots in green and gray indicate hDKK1C2 models in the complex and free form, respectively.

Table 4 The weak hydrogen bonds observed in the equilibrium state. The averaged atomic distances, and their standard deviation (S.D.) are shown along with the min/max distances observed in MD simulation on the complex models of hDKK1C2–hLRP6PD1 (A) and hDKK1C2–hLRP5PD1 (B). The values shown are in Å.

A

hDKK1C2–hLRP6PD1	Average	S.D.	Min.	Max.
Y238OH–P225O	4.05	0.97	2.57	7.01
R224N–R29NH1	4.08	0.12	3.05	5.41
Q235OE1–S267OG	4.09	0.17	3.08	5.34
K249NZ–N117OD1	4.14	1.01	2.58	7.36
S192N–S243O	4.17	0.14	3.07	5.31
R203NH1–I265O	4.22	0.15	2.93	5.65
H266ND1–E159N	4.25	0.53	2.81	6.15
R203NH1–F266N	4.27	0.26	3.10	6.17
L231O–D30OD2	4.42	0.26	3.17	5.92
L231O–D30OD1	4.43	0.53	2.98	7.01
C245O–W157NE1	4.48	0.36	3.20	5.97
H261NE2–E115OE1	4.48	0.14	2.75	5.53
H266NE2–G158O	4.49	0.44	2.95	6.51
R246NE–Q139NE2	4.52	0.31	3.09	6.22
K222O–R29NH1	4.62	0.26	2.95	6.25
R246NE–Q139OE1	4.64	0.63	2.95	7.11
K222NZ–E115OE1	4.68	0.15	2.82	5.62
S192OG–S243OG	4.70	0.69	2.55	6.86
R203NE–D264O	4.91	0.62	3.12	7.45
R246NH2–E136OE1	4.91	3.00	2.63	11.23
R246NH2–N117OD1	5.10	2.93	2.68	9.12
G240O–K202NZ	5.10	0.25	2.66	6.69
R246NH2–N117ND2	5.20	2.44	2.90	8.54
R246NH1–Q139NE2	5.23	1.50	2.94	8.12
R246NH2–E136O	5.28	1.16	2.69	7.99
K249NZ–T116O	5.42	0.86	3.03	7.99
R203NH2–D264OD1	5.43	0.66	2.75	7.86
K226NZ–E51OE1	5.46	5.23	2.60	12.55
K222NZ–E115OE2	5.56	0.19	2.89	6.73
K249NZ–E136OE1	5.60	3.21	2.60	10.34
K226NZ–E51OE2	5.76	4.12	2.54	11.58
K208NZ–S246OG	5.77	0.44	3.10	7.61
R246NH1–E136O	5.80	0.76	2.85	8.02
R246NH2–E136OE2	5.81	1.78	2.70	10.06
R246NH2–Q139OE1	6.12	1.48	3.10	8.71
R246NH1–E136OE1	6.18	2.77	2.69	11.63
R259NH2–VAL90O	6.37	1.71	3.19	9.26
K226NZ–S71OG	6.79	4.71	2.74	13.49
R259NH1–VAL90O	7.02	2.29	3.17	9.45
K208NZ–D264OD1	7.25	4.12	3.18	12.03
K208NZ–D264OD2	7.44	2.71	3.16	11.35
K249NZ–VAL91O	7.60	2.31	3.06	11.41

B

hDKK1C2–hLRP5PD1	Average	S.D.	Min.	Max.
G230O–W255NE1	4.17	0.47	2.81	6.18
S228O–S280OG	4.20	0.17	3.10	6.15
F205N–Y195OH	4.25	0.16	3.14	6.18
H229NE2–Q256OE1	4.33	1.42	2.61	7.97
K226NZ–D64OD2	4.43	1.89	2.60	8.13
S228O–R258NH2	4.43	0.44	2.75	6.42
H229NE2–Q256O	4.45	1.96	2.79	8.77
S228OG–Y279OH	4.60	0.48	3.12	7.32
H229NE2–W255O	4.63	0.49	2.84	7.04
K226NZ–D64OD1	4.99	2.44	2.55	8.61
K208NZ–E172OE2	5.21	3.23	2.60	9.25
K208NZ–E172OE1	5.25	2.67	2.63	9.08
Q235OE1–Y195OH	5.46	0.48	2.94	7.53
G227O–Y279OH	5.68	3.39	2.87	10.46
K226NZ–E63OE2	6.63	3.42	2.84	10.93
K226NZ–E63OE1	7.06	2.55	2.63	11.51
K226NZ–Y279OH	8.02	5.17	2.80	13.83
G230O–W255NE1	4.17	0.47	2.81	6.18

Unit is Å.

revealed that FL1 is responsible for intermolecular HBN. Judging from the findings above, we speculated that the conserved insertion in DKK3 impairs the interaction with LRP5/6. To confirm our hypothesis, we built an additional model of hDKK3C2 that lacks the unique insertion (hDKK3C2Δ). Since the same template (PDB: 2JTK) was employed for homology modeling of hDKK1C2 and hDKK3C2Δ, there was no marked difference in modeling structure between them except for the FL1 region. 5-ns MD simulation of the hDKK3C2Δ model was performed to refine the homology model. The final structure was used for docking simulation of hDKK3C2Δ to PD models of hLRP5. Among the binding poses generated by the docking

simulation, the complex model was selected base on the predicted binding affinity and the resemblance to the hDKK1C2–hLRP5PD1 complex structure. This enabled us to draw an adequate comparison between hDKK1C2 and hDKK3C2Δ. $\Delta G_{binding}$ was computed in the same manner. $\Delta G_{binding}$ values are shown in Table 5. Among the corresponding complexes, $\Delta G_{binding}$ values of hDKK3C2Δ were lower than those of hDKK3C2 (Table 2A). This means that the affinities of hDKK3C2Δ to hLRP5 will be slightly stronger than those of the wild-type hDKK3. In particular, $\Delta G_{binding}$ values of hDKK3C2Δ–hLRP5PD1 model (−40.6 kcal/mol) and hDKK3C2Δ–hLRP5PD2 model (−39.8 kcal/mol) imply that the affinities were moderately increased by deletion of the conserved region.

Additionally, we focused on P258 of hDKK3, which is adjacent to the C-terminal end of the conserved insertion, because P258 has a potential role in restriction of the FL1 conformation and thus a potential effect on the binding affinity for the receptors. A P258G mutation model of hDKK3C2Δ (hDKK3C2Δ P258G) was built in the same manner as used for the modeling procedure. FL1 in hDKK3C2ΔP258G was untwisted. Then hDKK3C2ΔP258G was docked to the PD models of hLRP5. The results of the affinity estimation are shown in Table 5. It should be noted that $\Delta G_{binding}$ of the hDKK3C2ΔP258G model to the hLRP5PD2 model was −48.9 kcal/mol. This result indicates that hDKK3C2ΔP258G had sufficiently high affinity to bind to the receptor, because the $\Delta G_{binding}$ values indicated similar levels of affinity between the hDKK1C2–hLRP5PD1 model (−47.7 kcal/mol) and hDKK1C2–hLRP6PD3 model (−48.0 kcal/mol). The above findings support our hypothesis.

As for FL2, the amino acid sequence was not conserved and a large variation was seen among the DKK family members (Fig . 3). The hydrogen bond analysis in Table 3 shows that no stable hydrogen bond

from FL2 was observed in either the complex models of hDKK1C2–hLRP6PD1 or hDKK1C2–hLRP5PD1. Accordingly, we considered that the FL2 region scarcely contributes to binding of the DKK2 protein to the β-propeller domains of LRP5/6. In this work, we mainly focused on the FL1 region and no supplementary computational analysis was performed for FL2.

Discussion

A series of molecular modelings including PPD simulations reproduced the following 4 key experimental observations: i) both DKK1 and DKK2 are ligands with high affinity to LRP5/6, ii) DKK4 also binds to the receptor, but the affinity is weaker than those of DKK1 and DKK2, iii) the binding modes found in the X-ray structures of hDKK1C2–hLR-P6PD3 (PDB code: 3S2K, 3S8V) show the importance of FL1 for interaction of the complex; and iv) DKK3 does not bind to the receptors. Furthermore, the binding modes found in the X-ray structures of hDKK1C2–hLRP6PD3 (PDB code: 3S2K and 3S8V) were similar to our predicted complex model (Cα RMS deviation $\cong 4\,\text{Å}$). Judging from the accordance with the experimental results, we concluded that our approach can provide an appropriate prediction for the complex structures and affinity profiles.

In the dynamic structure of the hDKK1C2–hLR-P6PD1 complex model, the hydrogen bonds involved in the stabilized regions in hDKK1C2 (C195–H204, S207–R225 and R236–Q253) significantly contribute to the affinity of the complex. One of the stabilized regions, C195–H204, is responsible for 5 stable hydrogen bonds with LRP6PD1. In addition, S207–R225 and R236–Q253 involve nine and 6 hydrogen bonds, respectively. Based on the occurrence of HBN, the contact of FL1 in hDKK1C2 is a significant factor underlying the physical recognition of hLRP6. Additionally, hydrogen bonds between Ser192OG in hDKK1C2 and Ser243OG in hLRP6PD1 were observed in the MD simulation of the complex model (Table 4A). As described in the previous section, in the complex model by PPD, the hydroxyl group of Ser243 interacted with the main-chain nitrogen atom of the other residue (Cys201). The change in the hydrogen bond network resulted from structural refinement by the MD simulation. Chen *et al.* reported that a mDKK1 mutant, H267E, attenuates the binding

Table 5   Affinity profile of mutant models of C2 hDKK3 (see text for details) for PD models of hLRP5. The values are in kcal/mol.

$\Delta G_{binding}$*	hDKK3C2Δ	hDKK3C2ΔP258G
hLRP5PD1	−40.57	−41.43
hLRP5PD2	−39.75	−48.90
hLRP5PD3	−28.89	−28.07
hLRP5PD4	−32.52	−44.58

The values are in kcal/mol.

affinity for mLRP6 [24]. In hDKK1, the sequence of amino acid residues corresponds to H261. In our MD simulation of hDKK1C2–hLRP6PD1 complex model, a weak hydrogen bond between H261NE2 in hDKK1C2 and E115OE1 in hLRP6PD1 was observed (Table 4A). Hence, the results of the simulation are also consistent with LRP6-binding deficiency in the H267E mutant of mDKK1.

It was found from the MD simulation of complex models of hDKK1C2–hLRP5PD1 and hDKK1C2–hLRP6PD1 that R203, K222, K226 and Q235 in hDKK1C2 produce stable intermolecular hydrogen bonds in both complex models and that 3 residues (K222, K226 and Q235) are part of the FL1 region. Therefore, we can conclude that FL1 is the most important factor for the receptor recognition. G171V located on hLRP5PD1 is genetically linked to high bone-mass [30, 36]. Therefore, G171 is considered to be involved in recognition of the DKK protein. In the MD simulation, a hydrogen bond was detected between the backbone oxygen atom of G171 and the guanidinium group of R203 in hDKK1C2 (Table 3B). Mutation of glycine to valine may disturb the approach of the side chain of R203 due to its hydrophobicity. Hence, it is thought that the G171V mutation on hLRP5 reduces the affinity for hDKK1 due to loss of the hydrogen bond with R203 in hDKK1C2. Since the first report on G171 mutation, several mutations have been reported to be related to osteogenic disorders, including D111Y, G171R, A214T/V, A242T and T253I [37]. Furthermore, A65V, S127V, L200V and M282V have also been reported to be potential disease-causing mutations because they are positioned at equivalent sites of G171 in each blade-propeller of LRP5PD1, and all of the mutant proteins have no WNT signaling activity due to a lack of affinity for DKK proteins [34]. At least in our MD simulation, however, direct interactions between the residues at the mutation sites described above and the residues in hDKK1C2 models were not found throughout the entire duration of MD simulation. Therefore, these mutants may have impaired function due to different factors, such as irrecoverable failure in the protein folding or a drastic change in the whole structure of the ligand binding site.

Based on the results of molecular simulation and a comparison with the results of experimental studies, we propose a novel hypothesis wherein the conserved 7-amino-acid insertion and P258 in DKK3 cooperatively lead to the lower binding affinity for LRP5/6. This means that the 7-amino-acid insertion and the substitution to proline may be evolutionarily critical for the birth of DKK3 from the ancestral gene of the DKK family. The unique sequence in DKK3 may be a driving force for the acquisition of intrinsic biological functions, such as tumoricidal effects and anti-tumor immune response [58]. It remains an open question why the insertion sequence (LDLITWE) is perfectly conserved between human and mouse DKK3. According to the orthologous gene database, Evola [59], the conservation is not only observed in humans and mice but also in *Pan troglodytes, Macaca mulatta, Rattus norvegicus, Canis familiaris, Equus caballus, Bos taurus, and Monodelphis domestica*. Interestingly, the DKK3 genes among more remotely related species encode slightly changed variants, such as *Gallus gallus* (LNLITWE), *Danio rerio* (MEVLLWE), *Oryzias latipes* (MDMLAWD) and *Takifugu rubripes* (MDMLAWD). Comparative analysis of the species indicates the presence of a sequence motif of 7 amino acids as follows. The motif starts with methionine or leucine. The second position is of acid type (D/E), the fourth position is leucine or isoleucine, the sixth is always tryptophan, and the seventh is an acidic residue again. We believe that the conserved residues are not only responsible for the inaccessibility to LRP5/6 but also have an important role for the specific recognition by a canonical receptor for DKK3.

The biological function of the inserted sequence of DKK3 has not been reported yet. So far, three potential candidates for DKK3 receptors have been independently reported. One of the candidates is β-TrCP1 (β-transduction repeat-containing protein), which is involved in the ubiquitin-mediated protein degradation pathway [60]. This receptor candidate was detected by yeast-two-hybrid (Y2H) screening for a DKK3 receptor. It should be noted that β-TrCP1 is usually localized in the cytoplasm, while the gene product of DKK3 is secreted into the extracellular space. Interestingly, it was experimentally confirmed that the DKK3 protein is expressed in the cytoplasm. The DKK3 in the cytoplasm can be translated from an alternative splicing mRNA isoform that lacks the coding region of signal sequences for destination to the endoplasmic reticulum. In fact, an mRNA variant of the DKK3 that lacks the signal sequence has been

cloned (AK092979) [61]. The variant form of DKK3 protein is spatially localized in the cytoplasm and interacts with β-TrCP1. X-ray crystallographic analysis revealed that β-TrCP1 has a β-propeller domain (PDB code: 1P22) [62]. From the structural analysis, it can be hypothesized that cytoplasmic DKK3 interacts with the β-propeller domain by the C2 domain, because DKK1/2/4 also targets a propeller-shaped structure. However, this hypothesis is only based on structural analogy. Hence, further analysis is required. Kremen-1/2 have been reported to be novel binding partners of DKK3 [63]. Kremen-1/2 are secreted-type proteins that are involved in WNT signaling, and therefore are potential candidates for the binding partner of the secreted form of DKK3. Unfortunately, three-dimensional structures of the Kremen proteins have not yet been clarified. When structural information on the receptor becomes available, it will be very helpful to examine the physico-chemical interaction with DKK3. Finally, the use of a combination of Y2H and a mammalian two-hybrid system revealed Tctex-1 as a potential candidate for the receptor for hDKK3 [64]. The experimental results thus indicate a variety of functions of DKK3.

In this study, PPD simulation was performed by ZDOCK and affinity estimation was executed by the RDOCK/CHARMM system. It should be noted that ZDOCK employs a rigid docking algorithm. Also, there is currently no optimal scoring function that correctly predicts the experimentally determined affinities [65]. In a future study, the prediction strategy should be improved by combined use of flexible docking and a more efficient scoring function.

In conclusion, The reason why DKK3 does not interact with LRP5/6 was clarified by comparing structural properties of complex models consisting of high-affinity ligands and receptors. We found from the simulation that the affinity between C2 and PD domains strongly depends on interaction with the FL1 region in the C2 domain. However, in DKK3, longer FL1 including a unique inserted sequence (LDLITWE) disturbs proper interaction with PD domains. The conformational restriction of FL1 caused by P258 is also thought to influence the affinity. The sequences and structural property unique to the C2 domain found in DKK3 might be a key for identifying its receptor.

References

1. Tsuji T, Miyazaki M, Sakaguchi M, Inoue Y and Namba M: A REIC gene shows down-regulation in human immortalized cells and human tumor-derived cell lines. Biochem Biophys Res Commun (2000) 268: 20–24.

2. Tsuji T, Nozaki I, Miyazaki M, Sakaguchi M, Pu H, Hamazaki Y, Iijima O and Namba M: Antiproliferative activity of REIC/Dkk-3 and its significant down-regulation in non-small-cell lung carcinomas. Biochem Biophys Res Commun (2001) 289: 257–263.

3. Kobayashi K: Reduced expression of the REIC/Dkk-3 gene by promoter-hypermethylation in human tumor cells. Gene (2002) 282: 151–158.

4. Hsieh SY, Hsieh PS, Chiu CT and Chen WY: Dickkopf-3/REIC functions as a suppressor gene of tumor growth. Oncogene (2004) 23: 9183–9189.

5. Kurose K, Sakaguchi M, Nasu Y, Ebara S, Kaku H, Kariyama R, Arao Y, Miyazaki M, Tsushima T, Namba M, Kumon H and Huh N-H: Decreased expression of REIC/Dkk-3 in human renal clear cell carcinoma. J Urol (2004) 171: 1314–1318.

6. Roman-Gomez J, Jimenez-Velasco A, Agirre X, Castillejo JA, Navarro G, Barrios M, Andreu EJ, Prosper F, Heiniger A and Torres A: Transcriptional silencing of the Dickkopfs-3 (Dkk-3) gene by CpG hypermethylation in acute lymphoblastic leukaemia. Brit J Cancer (2004) 91: 707–713.

7. Kuphal S, Lodermeyer S, Bataille F, Schuierer M, Hoang BH and Bosserhoff AK: Expression of Dickkopf genes is strongly reduced in malignant melanoma. Oncogene (2006) 25: 5027–5036.

8. Urakami S, Shiina H, Enokida H, Kawakami T, Kawamoto K, Hirata H, Tanaka Y, Kikuno N, Nakagawa M, Igawa M and Dahiya R: Combination analysis of hypermethylated Wnt-antagonist family genes as a novel epigenetic biomarker panel for bladder cancer detection. Clin Cancer Res (2006) 12: 2109–2116.

9. Zitt M, Untergasser G, Amberger A, Moser P, Stadlmann S, Muller HM, Muhlmann G, Perathoner A, Margreiter R, Gunsilius E and Ofner D: Dickkopf-3 as a new potential marker for neoangiogenesis in colorectal cancer: expression in cancer tissue and adjacent non-cancerous tissue. Dis Markers (2008) 24: 101–109.

10. Chen J, Watanabe M, Huang P, Sakaguchi M, Ochiai K, Nasu Y, Ouchida M, Huh NH, Shimizu K, Kashiwakura Y, Kaku H and Kumon H: REIC/Dkk-3 stable transfection reduces the malignant phenotype of mouse prostate cancer RM9 cells. Int J Mol Med (2009) 24: 789–794.

11. Ding Z, Qian YB, Zhu LX and Xiong QR: Promoter methylation and mRNA expression of DKK-3 and WIF-1 in hepatocellular carcinoma. World J Gastroenterol (2009) 15: 2595–2601.

12. Fong D, Hermann M, Untergasser G, Pirkebner D, Draxl A, Heitz M, Moser P, Margreiter R, Hengster P and Amberger A: Dkk-3 expression in the tumor endothelium: a novel prognostic marker of pancreatic adenocarcinomas. Cancer Sci (2009) 100: 1414–1420.

13. Zhang K, Watanabe M, Kashiwakura Y, Li S, Edamura K, Huang P, Yamaguchi K, Nasu Y, Kobayashi Y, Sakaguchi M, Ochiai K, Yamada H, Takei K, Ueki H, Huh N, Li M, Kaku H, Na Y and Kumon H: Expression

pattern of REIC/Dkk-3 in various cell types and the implications of the soluble form in prostatic acinar development. Int J Oncol (2010) 37: 1495–1501.

14. Abarzua F, Sakaguchi M, Takaishi M, Nasu Y, Kurose K, Ebara S, Miyazaki M, Namba M, Kumon H and Huh N-h: Adenovirus-mediated overexpression of REIC/Dkk-3 selectively induces apoptosis in human prostate cancer cells through activation of c-Jun-NH2-kinase. Cancer Res (2005) 65: 9617–9622.

15. Tanimoto R, Abarzua F, Sakaguchi M, Takaishi M, Nasu Y, Kumon H and Huh NH: REIC/Dkk-3 as a potential gene therapeutic agent against human testicular cancer. Int J Mol Med (2007) 19: 363–368.

16. Kobayashi T, Sakaguchi M, Tanimoto R, Abarzua F, Takaishi M, Kaku H, Kataoka K, Saika T, Nasu Y, Miyazaki M, Kumon H and Huh NH: Mechanistic analysis of resistance to REIC/Dkk-3-induced apoptosis in human bladder cancer cells. Acta Med Okayama (2008) 62: 393–401.

17. Kawasaki K, Watanabe M, Sakaguchi M, Ogasawara Y, Ochiai K, Nasu Y, Doihara H, Kashiwakura Y, Huh NH, Kumon H and Date H: REIC/Dkk-3 overexpression downregulates P-glycoprotein in multidrug-resistant MCF7/ADR cells and induces apoptosis in breast cancer. Cancer Gene Ther (2009) 16: 65–72.

18. Sakaguchi M, Kataoka K, Abarzua F, Tanimoto R, Watanabe M, Murata H, Than SS, Kurose K, Kashiwakura Y, Ochiai K, Nasu Y, Kumon H and Huh N-h: Overexpression of REIC/Dkk-3 in normal fibroblasts suppresses tumor growth via induction of interleukin-7. J Biol Chem (2009) 284: 14236–14244.

19. Watanabe M, Kashiwakura Y, Huang P, Ochiai K, Futami J, Li S-A, Takaoka M, Nasu Y, Sakaguchi M, Huh N-H and Kumon H: Immunological aspects of REIC/Dkk-3 in monocyte differentiation and tumor regression. Int J Oncol (2009) 34: 657–663.

20. Brott BK and Sokol SY: Regulation of Wnt/LRP signaling by distinct domains of Dickkopf proteins. Mol Cell Biol (2002) 22: 6100–6110.

21. Fujita K and Janz S: Attenuation of WNT signaling by DKK-1 and -2 regulates BMP2-induced osteoblast differentiation and expression of OPG, RANKL and M-CSF. Mol Cancer (2007) 6: 71.

22. Li L, Mao JH, Sun L, Liu WZ and Wu DQ: Second cysteine-rich domain of Dickkopf-2 activates canonical Wnt signaling pathway via LRP-6 independently of dishevelled. J Biol Chem (2002) 277: 5977–5981.

23. Mao BY and Niehrs C: Kremen2 modulates Dickkopf2 activity during Wnt/LRP6 signaling. Gene (2003) 302: 179–183.

24. Chen L, Wang K, Shao Y, Huang J, Li X, Shan J, Wu D and Zheng JJ: Structural insight into the mechanisms of Wnt signaling antagonism by Dkk. J Biol Chem (2008) 283: 23364–23370.

25. Mao B, Wu W, Li Y, Hoppe D, Stannek P, Glinka A and Niehrs C: LDL-receptor-related protein 6 is a receptor for Dickkopf proteins. Nature (2001) 411: 321–325.

26. Kato M, Patel MS, Levasseur R, Lobov I, Chang BHJ, Glass DA, Hartmann C, Li L, Hwang TH, Brayton CF, Lang RA, Karsenty G and Chan L: Cbfa1-independent decrease in osteoblast proliferation, osteopenia, and persistent embryonic eye vascularization in mice deficient in Lrp5, a Wnt coreceptor. J Cell Biol (2002) 157: 303–314.

27. Ferrari SL, Deutsch S, Choudhury U, Chevalley T, Bonjour JP, Dermitzakis ET, Rizzoli R and Antonarakis SE: Polymorphisms in the low-density lipoprotein receptor-related protein 5 (LRP5) gene are associated with variation in vertebral bone mass, vertebral bone size, and stature in whites. Am J Hum Genet (2004) 74: 866–875.

28. Little RD, Recker RR and Johnson ML: High bone density due to a mutation in LDL-receptor-related protein 5. N Engl J Med (2002) 347: 943–943.

29. Gong Y, Slee RB, Fukai N, Rawadi G, Roman-Roman S, Reginato AM, Wang HW, Cundy T, Glorieux FH, Lev D, Zacharin M, Oexle K, Marcelino J, Suwairi W, Heeger S, Sabatakos G, Apte S, Adkins WN, Allgrove J, Arslan-Kirchner M, Batch JA, Beighton P, Black GCM, Boles RG, Boon LM, Borrone C, Brunner HG, Carle GF, Dallapiccola B, De Paepe A, Floege B, Halfhide ML, Hall B, Hennekam RC, Hirose T, Jans A, Juppner H, Kim CA, Keppler-Noreuil K, Kohlschuetter A, LaCombe D, Lambert M, Lemyre E, Letteboer T, Peltonen L, Ramesar RS, Romanengo M, Somer H, Steichen-Gersdorf E, Steinmann B, Sullivan B, Superti-Furga A, Swoboda W, van den Boogaard MJ, Van Hul W, Vikkula M, Votruba M, Zabel B, Garcia T, Baron R, Olsen BR, Warman ML and Osteoporosis Pseudoglioma S: LDL receptor-related protein 5 (LRP5) affects bone accrual and eye development. Cell (2001) 107: 513–523.

30. Boyden LM, Mao JH, Belsky J, Mitzner L, Farhi A, Mitnick MA, Wu DQ, Insogna K and Lifton RP: High bone density due to a mutation in LDL-receptor-related protein 5. New Engl J Med (2002) 346: 1513–1521.

31. Levasseur R, Lacombe D and de Vernejoul MC: LRP5 mutations in osteoporosis-pseudoglioma syndrome and high-bone-mass disorders. Joint Bone Spine (2005) 72: 207–214.

32. Pinson KI, Brennan J, Monkley S, Avery BJ and Skarnes WC: An LDL-receptor-related protein mediates Wnt signalling in mice. Nature (2000) 407: 535–538.

33. Mani A, Radhakrishnan J, Wang H, Mani MA, Nelson-Williams C, Carew KS, Mane S, Najmabadi H, Wu D and Lifton RP: LRP6 mutation in a family with early coronary disease and metabolic risk factors. Science (2007) 315: 1278–1282.

34. Bhat BM, Allen KM, Liu W, Graham J, Morales A, Anisowicz A, Lam H-S, McCauley C, Coleburn V, Cain M, Fortier E, Bhat RA, Bex FJ and Yaworsky PJ: Structure-based mutation analysis shows the importance of LRP5 beta-propeller 1 in modulating Dkk1-mediated inhibition of Wnt signaling. Gene (2007) 391: 103–112.

35. Binnerts ME, Tomasevic N, Bright JM, Leung J, Ahn VE, Kim KA, Zhan XM, Liu SC, Yonkovich S, Williams J, Zhou M, Gros D, Dixon M, Korver W, Weis WI and Abo A: The First Propeller Domain of LRP6 Regulates Sensitivity to DKK1. Mol Biol Cell (2009) 20: 3552–3560.

36. Little RD, Carulli JP, Del Mastro RG, Dupuis J, Osborne M, Folz C, Manning SP, Swain PM, Zhao SC, Eustace B, Lappe MM, Spitzer L, Zweier S, Braunschweiger K, Benchekroun Y, Hu XT, Adair R, Chee L, FitzGerald MG, Tulig C, Caruso A, Tzellas N, Bawa A, Franklin B, McGuire S, Nogues X, Gong G, Allen KM, Anisowicz A, Morales AJ, Lomedico PT, Recker SM, Van Eerdewegh P, Recker RR and Johnson ML: A mutation in the LDL receptor-related protein 5 gene results in the autosomal dominant high-bone-mass trait. Am J Hum Genet (2002) 70: 11–19.

37. Van Wesenbeeck L, Cleiren E, Gram J, Beals RK, Benichou O, Scopelliti D, Key L, Renton T, Bartels C, Gong YQ, Warman ML, de Vernejoul MC, Bollerslev J and Van Hul W: Six novel missense mutations in the LDL receptor-related protein 5 (LRP5) gene in different conditions with an increased bone density. Am J Hum Genet (2003) 72: 763–771.

38. Cheng Z, Biechele T, Wei ZY, Morrone S, Moon RT, Wang LG and Xu WQ: Crystal structures of the extracellular domain of LRP6 and its complex with DKK1. Nat Struct Mol Biol (2011) 18: 1204–1210.

39. Ahn VE, Chu MLH, Choi HJ, Tran D, Abo A and Weis WI: Structural Basis of Wnt Signaling Inhibition by Dickkopf Binding to LRP5/6. Dev Cell (2011) 21: 862–873.

40. Jeon H, Meng W, Takagi J, Eck MJ, Springer TA and Blacklow SC: Implications for familial hypercholesterolemia from the structure of the LDL receptor YWTD-EGF domain pair. Nat Struct Biol (2001) 8: 499–504.

41. Imanishi T, Itoh T, Suzuki Y, O'Donovan C, Fukuchi S, Koyanagi KO, Barrero RA, Tamura T, Yamaguchi-Kabata Y, Tanino M, Yura K, Miyazaki S, Ikeo K, Homma K, Kasprzyk A, Nishikawa T, Hirakawa M, Thierry-Mieg J, Thierry-Mieg D, Ashurst J, Jia L, Nakao M, Thomas MA, Mulder N, Karavidopoulou Y, Jin L, Kim S, Yasuda T, Lenhard B,

Eveno E, Suzuki Y, Yamasaki C, Takeda J-i, Gough C, Hilton P, Fujii Y, Sakai H, Tanaka S, Amid C, Bellgard M, Bonaldo MdF, Bono H, Bromberg SK, Brookes AJ, Bruford E, Carninci P, Chelala C, Couillault C, de Souza SJ, Debily M-A, Devignes M-D, Dubchak I, Endo T, Estreicher A, Eyras E, Fukami-Kobayashi K, Gopinath GR, Graudens E, Hahn Y, Han M, Han Z-G, Hanada K, Hanaoka H, Harada E, Hashimoto K, Hinz U, Hirai M, Hishiki T, Hopkinson I, Imbeaud S, Inoko H, Kanapin A, Kaneko Y, Kasukawa T, Kelso J, Kersey P, Kikuno R, Kimura K, Korn B, Kuryshev V, Makalowska I, Makino T, Mano S, Mariage-Samson R, Mashima J, Matsuda H, Mewes H-W, Minoshima S, Nagai K, Nagasaki H, Nagata N, Nigam R, Ogasawara O, Ohara O, Ohtsubo M, Okada N, Okido T, Oota S, Ota M, Ota T, Otsuki T, Piatier-Tonneau D, Poustka A, Ren S-X, Saitou N, Sakai K, Sakamoto S, Sakate R, Schupp I, Servant F, Sherry S, Shiba R, Shimizu N, Shimoyama M, Simpson AJ, Soares B, Steward C, Suwa M, Suzuki M, Takahashi A, Tamiya G, Tanaka H, Taylor T, Terwilliger JD, Unneberg P, Veeramachaneni V, Watanabe S, Wilming L, Yasuda N, Yoo H-S, Stodolsky M, Makalowski W, Go M, Nakai K, Takagi T, Kanehisa M, Sakaki Y, Quackenbush J, Okazaki Y, Hayashizaki Y, Hide W, Chakraborty R, Nishikawa K, Sugawara H, Tateno Y, Chen Z, Oishi M, Tonellato P, Apweiler R, Okubo K, Wagner L, Wiemann S, Strausberg RL, Isogai T, Auffray C, Nomura N, Gojobori T and Sugano S: Integrative annotation of 21,037 human genes validated by full-length cDNA clones. PLoS Biol (2004) 2: e162.

42. Yamasaki C, Murakami K, Takeda J-i, Sato Y, Noda A, Sakate R, Habara T, Nakaoka H, Todokoro F, Matsuya A, Imanishi T and Gojobori T: H-InvDB in 2009: extended database and data mining resources for human genes and transcripts. Nucleic Acids Res (2010) 38: D626–632.

43. UniProt C: The Universal Protein Resource (UniProt) in 2010. Nucleic Acids Res (2010) 38: D142–D148.

44. Sali A and Blundell TL: Comparative protein modelling by satisfaction of spatial restraints. J Mol Biol (1993) 234: 779–815.

45. Fiser A, Do RK and Sali A: Modeling of loops in protein structures. Protein Sci (2000) 9: 1753–1773.

46. Shen M-Y and Sali A: Statistical potential for assessment and prediction of protein structures. Protein Sci (2006) 15: 2507–2524.

47. Jorgensen WL, Chandrasekhar J, Madura JD, Impey RW and Klein ML: Comparison of simple potential functions for simulating liquid water. J Chem Phys (1983) 79: 926–935.

48. Cheatham TE III, Miller JL, Fox T, Darden TA and Kollman PA: Molecular Dynamics Simulations on Solvated Biomolecular Systems: The Particle Mesh Ewald Method Leads to Stable Trajectories of DNA, RNA, and Proteins. J Am Chem Soc (1995) 117: 4193–4194.

49. Darden T, Perera L, Li LP and Pedersen L: New tricks for modelers from the crystallography toolkit: the particle mesh Ewald algorithm and its use in nucleic acid simulations. Structure (1999) 7: R55–R60.

50. Chen R, Li L and Weng Z: ZDOCK: an initial-stage protein-docking algorithm. Proteins (2003) 52: 80–87.

51. Li L, Chen R and Weng ZP: RDOCK: Refinement of rigid-body protein docking predictions. Proteins (2003) 53: 693–707.

52. Zhang C, Vasmatzis G, Cornette JL and DeLisi C: Determination of atomic desolvation energies from the structures of crystallized proteins. J Mol Biol (1997) 267: 707–726.

53. Sanner MF, Olson AJ and Spehner JC: Reduced surface: An efficient way to compute molecular surfaces. Biopolymers (1996) 38: 305–320.

54. Larkin MA, Blackshields G, Brown NP, Chenna R, McGettigan PA, McWilliam H, Valentin F, Wallace IM, Wilm R, Lopez R, Thompson JD, Gibson TJ and Higgins DG: Clustal W and clustal X version 2.0. Bioinformatics (2007) 23: 2947–2948.

55. Kaminuma E, Mashima J, Kodama Y, Gojobori T, Ogasawara O, Okubo K, Takagi T and Nakamura Y: DDBJ launches a new archive database with analytical tools for next-generation sequence data. Nucleic Acids Res (2010) 38: D33–D38.

56. Binnerts ME, Tomasevic N, Bright JM, Leung J, Ahn VE, Kim K-A, Zhan X, Liu S, Yonkovich S, Williams J, Zhou M, Gros D, Dixon M, Korver W, Weis WI and Abo A: The first propeller domain of LRP6 regulates sensitivity to DKK1. Mol Biol Cell (2009) 20: 3552–3560.

57. Lo Conte L, Chothia C and Janin J: The atomic structure of protein-protein recognition sites. J Mol Biol (1999) 285: 2177–2198.

58. Veeck J and Dahl E: Targeting the Wnt pathway in cancer: The emerging role of Dickkopf-3. Biochim Et Biophys Acta (2012) 1825: 18–28.

59. Matsuya A, Sakate R, Kawahara Y, Koyanagi KO, Sato Y, Fujii Y, Yamasaki C, Habara T, Nakaoka H, Todokoro F, Yamaguchi K, Endo T, Oota S, Makalowski W, Ikeo K, Suzuki Y, Hanada K, Hashimoto K, Hirai M, Iwama H, Saitou N, Hiraki AT, Jin L, Kaneko Y, Kanno M, Murakami K, Noda AO, Saichi N, Sanbonmatsu R, Suzuki M, Takeda JI, Tanaka M, Gojobori T, Imanishi T and Itoh T: Evola: Ortholog database of all human genes in H-InvDB with manual curation of phylogenetic trees. Nucleic Acids Res (2008) 36: D787–D792.

60. Lee EJ, Jo M, Rho SB, Park K, Yoo YN, Park J, Chae M, Zhang W and Lee JH: Dkk3, downregulated in cervical cancer, functions as a negative regulator of beta-catenin. Int J Cancer (2009) 124: 287–297.

61. Ota T, Suzuki Y, Nishikawa T, Otsuki T, Sugiyama T, Irie R, Wakamatsu A, Hayashi K, Sato H, Nagai K, Kimura K, Makita H, Sekine M, Obayashi M, Nishi T, Shibahara T, Tanaka T, Ishii S, Yamamoto J, Saito K, Kawai Y, Isono Y, Nakamura Y, Nagahari K, Murakami K, Yasuda T, Iwayanagi T, Wagatsuma M, Shiratori A, Sudo H, Hosoiri T, Kaku Y, Kodaira H, Kondo H, Sugawara M, Takahashi M, Kanda K, Yokoi T, Furuya T, Kikkawa E, Omura Y, Abe K, Kamihara K, Katsuta N, Sato K, Tanikawa M, Yamazaki M, Ninomiya K, Ishibashi T, Yamashita H, Murakawa K, Fujimori K, Tanai H, Kimata M, Watanabe M, Hiraoka S, Chiba Y, Ishida S, Ono Y, Takiguchi S, Watanabe S, Yosida M, Hotuta T, Kusano J, Kanehori K, Takahashi-Fujii A, Hara H, Tanase T, Nomura Y, Togiya S, Komai F, Hara R, Takeuchi K, Arita M, Imose N, Musashino K, Yuuki H, Oshima A, Sasaki N, Aotsuka S, Yoshikawa Y, Matsunawa H, Ichihara T, Shiohata N, Sano S, Moriya S, Momiyama H, Satoh N, Takami S, Terashima Y, Suzuki O, Nakagawa S, Senoh A, Mizoguchi H, Goto Y, Shimizu F, Wakebe H, Hishigaki H, Watanabe T, Sugiyama A, Takemoto M, Kawakami B, Watanabe K, Kumagai A, Itakura S, Fukuzumi Y, Fujimori Y, Komiyama M, Tashiro H, Tanigami A, Fujiwara T, Ono T, Yamada K, Fujii Y, Ozaki K, Hirao M, Ohmori Y, Kawabata A, Hikiji T, Kobatake N, Inagaki H, Ikema Y, Okamoto S, Okitani R, Kawakami T, Noguchi S, Itoh T, Shigeta K, Senba T, Matsumura K, Nakajima Y, Mizuno T, Morinaga M, Sasaki M, Togashi T, Oyama M, Hata H, Komatsu T, Mizushima-Sugano J, Satoh T, Shirai Y, Takahashi Y, Nakagawa K, Okumura K, Nagase T, Nomura N, Kikuchi H, Masuho Y, Yamashita R, Nakai K, Yada T, Ohara O, Isogai T and Sugano S: Complete sequencing and characterization of 21,243 full-length human cDNAs. Nat Genet (2004) 36: 40–45.

62. Wu G, Xu GZ, Schulman BA, Jeffrey PD, Harper JW and Pavletich NP: Structure of a beta-TrCP1-Skp1-beta-catenin complex: Destruction motif binding and lysine specificity of the SCF beta-TrCP1 ubiquitin ligase. Mol Cell (2003) 11: 1445–1456.

63. Nakamura RE and Hackam AS: Analysis of Dickkopf3 interactions with Wnt signaling receptors. Growth Factors (2010) 28: 232–242.

64. Ochiai K, Watanabe M, Ueki H, Huang P, Fujii Y, Nasu Y, Noguchi H, Hirata T, Sakaguchi M, Huh N, Kashiwakura Y, Kaku H and Kumon H: Tumor suppressor REIC/Dkk-3 interacts with the dynein light chain, Tctex-1. Biochem Biophys Res Commun (2011) 412: 391–395.

65. Kastritis PL and Bonvin A: Are Scoring Functions in Protein-Protein Docking Ready To Predict Interactomes? Clues from a Novel Binding Affinity Benchmark. J Proteome Res (2010) 9: 2216–2225.